Paper393

Terrestrial Walking Robot With 2DoF Ionic Polymer–Metal Composite (IPMC) Legs

Kim Tien Nguyen, Seong Young Ko, Jong-Oh Park, and Sukho Park, *Member, IEEE*

***Abstract*—This paper proposes a terrestrial walking robot using ionic polymer–metal composite (IPMC) actuators based on a poly-vinylidene fluoride (PVDF)/polyvinyl pyrrolidone (PVP)/polystyrene sulfuric acid (PSSA) blend membrane. The IPMC based on PVDF/PVP/PSSA with a polymer mixture ratio of 30/15/55 shows a higher tip displacement and greater blocking force than Nafion-based IPMC actuators at low dc voltages. An actuation model is developed for the proposed membrane-based IPMC actuators, representing the transfer function between the input applied voltage and the output displacement of the IPMC actuator. For the terrestrial walking robot, we use a two-degrees-of-freedom (2DoF) leg structure because of its superior characteristics in comparison with a 1DoF leg structure. In addition, a kinematic model of the 2DoF leg structure is introduced as a modeling framework based on the actuation model for the analysis of the locomotion using this IPMC leg structure. The simulation results of the actuation model and the kinematic model are compared with the empirical response of 1 and 2DoF legs. A terrestrial walking robot (size: $28\ \mathrm{mm} \times 18\ \mathrm{mm} \times 16.5\ \mathrm{mm}$, weight: 1.2 g) with two 2DoF IPMC legs and two dummy legs has been designed and fabricated. Finally, we demonstrate the walking motion of the terrestrial walking robot.**

***Index Terms*—Biomimetic robot, ionic polymer–metal composite (IPMC), terrestrial walking robot, two-degrees-of-freedom (2DoF) leg.**

I. Introduction

As the demand for new materials to replace conventional materials such as metals and alloys, in the fields of biomimetics, robotics, electronics, automobiles, household goods, and medicine, electroactive polymers (EAPs) have appeared and are increasingly considered a promising smart material because of their tremendous advantages. As its name suggests, an EAP is a type of active polymer, which can change its shape and size in an electrical field. There are many different types of EAPs, but they can be divided into two categories: electronic EAPs and ionic EAPs. Ionic polymer–metal composites (IPMCs) form an important category of ionic EAPs, which is typically composed of a thin ion-exchange membrane (e.g., Nafion, or Flemion, etc.), which is chemically or physically composited with noble metal electrodes such as platinum, gold, and silver [1]. Under electrical field, the IPMC actuator shows a fast bending deformation toward the anode, due to the movement of the hydrated ions and cations toward the cathode [2]. On the other hand, the IPMC actuator generates an electrical charge at each side of the IPMC actuator when the mechanical deformation is applied [3]. The aforementioned explanations provide a compact view of fundamental principles of both actuation and sensing of the IPMC actuator [4].

The proposed IPMC actuator based on poly-vinylidene fluoride (PVDF)/polyvinyl pyrrolidone (PVP)/polystyrene sulfuric acid (PSSA) blend membrane has PSSA as a strong polyelectrolyte, which exhibits a high charge-carrier concentration (ion-exchange capacity around 4.4 mequiv.g^{-1}), and large volume of moving water [5]. With the ion-exchange process, the other electrolyte, LiCl, was used to replace positive hydrogen ions (H^+) by positive lithium ions (Li^+) for the increase of the membrane's conductivity. When the ionic polymer is hydrated, the cations (H^+ or Li^+) associated with the ${SO_3}^{-1}$ groups of PSSA become mobile, allowing the polymer to conduct cations while anions (negatively charged ions) are fixed to the ionic polymer membrane [2].

Generally, the IPMC actuator consists of biocompatible materials which are nontoxic and without damage to human body with a low actuation voltage [6]. Therefore, we expect that IPMC actuator can be suitable for medical application and our proposed walking robot can be applied in biomedical application that can diagnose and monitor digestive organs in humans.

Contrary to swimming motion, a walking motion is aimed at moving across many kinds of terrains, not only in aquatic environments but also in terrestrial environments. However, the main concern for a terrestrial walking robot is how to support and move the robot, especially a bio-inspired walking robot using IPMCs. Many researchers concentrated their efforts on the design of a walking robot structure and walking mechanism in order to apply this potential IPMC to the biomicrowalking robot. Chang *et al.* proposed an aquatic IPMC walking robot (size: $102\ \mathrm{mm} \times 80\ \mathrm{mm} \times 43$ mm, weight: 39 g) using six two-degrees-of-freedom (2DoF) legs and demonstrated a walking motion in water at the speed of 0.5 mm/s [7]. However, the legs of the walking robot were independently activated, which cannot demonstrate the best performance in terms of the blocking force and displacement of the 2DoF legs. Most of the walking robots using IPMC actuators adopted only one IPMC actuator as one leg (1DoF leg) [8]. We had already reported a micro terrestrial walking robot with four 1DoF legs using poly-vinylidene fluoride (PVDF)/polyvinyl pyrrolidone

Manuscript received October 27, 2014; revised January 29, 2015; accepted March 31, 2015. Date of publication June 9, 2015; date of current version October 21, 2015. Recommended by Technical Editor F. Carpi. This work was supported by the Basic Science Research Program through the National Research Foundation of Korea (NRF) funded by the Ministry of Education (2011-0009975). *(Corresponding authors: Jong-Oh Park and Sukho Park.)*

K. T. Nguyen and S. Y. Ko are with the School of Mechanical Engineering, Chonnam National University, Gwangju 500-757, Korea (e-mail: nguyenkimtien90@gmail.com; sko@jnu.ac.kr).

J.-O. Park and S. Park are with the School of Mechanical Engineering, Chonnam National University, Gwangju 500-757, Korea (e-mail: jop@jnu.ac.kr; spark@jnu.ac.kr).

Color versions of one or more of the figures in this paper are available online at http://ieeexplore.ieee.org.

Digital Object Identifier 10.1109/TMECH.2015.2419820

(PVP)/polystyrene sulfuric acid (PSSA)-based IPMC actuators, which demonstrated a successful locomotion of the walking robot (size: $18\,\mathrm{mm} \times 11\,\mathrm{mm} \times 12\,\mathrm{mm}$, weight: 1.3 g) [9]. However, the limitation of 1DoF legs is that they cannot control the motion curve of the leg. Therefore, the 1DoF leg cannot control the direction of the walking robot and can cause the slipping motion of the walking robot. Besides, in aquatic environments, the motion curve of the robot legs and the ground contact are not a primary concern because of the buoyancy in the surrounding water. In terrestrial environments, especially at a millimeter scale, where the friction force governs all the motions, the controllability of the motion curve of the legs plays a very important role in the design of the walking mechanism and the locomotion of the walking robot. Therefore, in this paper, a walking mechanism using 2DoF legs that is capable of controlling the leg's motion curve is designed. Finally, we first reported the dynamic model and kinematic model for the proposed 2DoF leg using PVDF/PVP/PSSA based IPMC actuator and demonstrated a terrestrial walking motion of the proposed walking robot using the 2DoF legs.

II. PVDF/PVP/PSSA-Based IPMC Actuator for a Terrestrial Walking Robot

A. Characterization of IPMC Properties

Many factors affected the IPMC actuator and caused its nonlinear behavior, such as membrane conditions, surface conditions, conductivity, size, and driving voltage. The ion-exchange membrane decides how much mobile cations and absorbed water molecules are included in the membrane of IPMC. By controlling the membrane condition, the characteristics and performance of IPMC can be generally identified. The proposed blend membrane based on PVDF/ PVP/PSSA with a ratio of 30/15/55 has shown better performance in comparison with a conventional Nafion-based membrane [2]. To prepare the blend membrane, the polymeric components such as PVDF, PVP in powder form and PSSA liquid form were dissolved with N, N dimethyl formamide (DMF) (Sigma Aldrich) to form a 10 w.t% membrane mixture solution. The electroless plating method was selected because of the non-conductivity properties of the proposed membrane. The following ingredients must be prepared, such as Tetra-ammine platinum (II) chloride hydrate ($[Pt(NH_3)_4]Cl_2 \times H_2O$)(Sigma Aldrich), sodium borohydride, lithium chloride, hydroxyl ammonium chloride, hydrochloric acid, and ammonium hydroxide (DAE-JUNG, Korea). IPMC fabrication procedures were taken from the previous works [2], [5], [10], [11] and they have been enhanced to ensure sufficient force and displacement for robotics applications. By applying voltage to the surface of the IPMC, the cations can be attracted, repelled, and cause the deflection of IPMC. Through the uniform surface layer thickness, low resistance, and high conductivity of the electrodes, IPMC can demonstrate a good performance. Through the repeated coating of the platinum electrodes, our fabrication method provided 10–20-μm platinum layers that increase the surface conductivity and reduce the surface resistance to 0.2 Ω/mm. Many experiments had been implemented to control the deflection of the IPMC strip by changing its size. The size could affect deflection due to stiffness, which can be changed by increasing or decreasing the thickness, length, and width. A thicker IPMC can generate a greater blocking force, but it is smaller in displacement. Similarly, when increasing the width or decreasing the length, the greater force and smaller displacement can be obtained. In this study, a $15\text{-mm} \times 4\text{-mm} \times 0.36\text{-mm}$ IPMC was chosen for the walking robot. Although a higher driving voltage can show a faster response, as well as a greater force and larger displacement, it can cause damage to the surface electrode, making electrolysis stronger and faster and reducing the lifetime of IPMC.

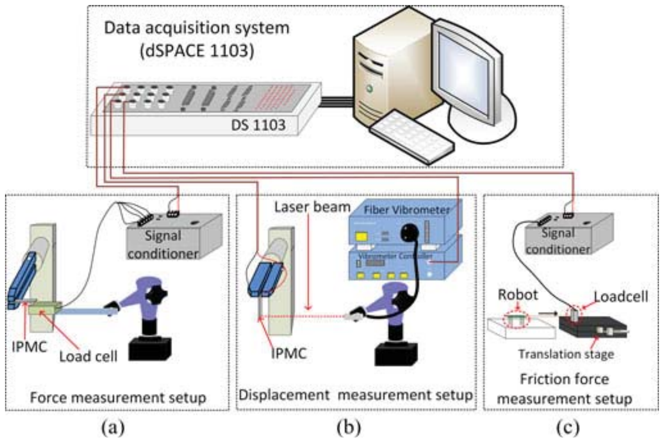

Fig. 1. Experimental setup for the IPMC bending test, blocking force test, friction force test, and propulsion force test.

In order to measure IPMC response performance, a data acquisition system was prepared and set up as in Fig. 1. A load cell (GSO-10, Transducer Techniques) with capacity of 10 gf and load cell signal conditioner (TMO-2, Transducer Techniques), for amplifying the signal from load cell to the measureable range (0–10 V), were used to measure the blocking force. The IPMC actuator was horizontally fixed to the clamping device and slightly touched the load cell as in Fig. 1(a). A laser vibrometer (Model No.-OFV-2510, Polytec) was used to record the tip displacement of IPMC actuator. The laser beam was fired and directed to the tip of the IPMC actuator via a fiber-optic cable [see Fig. 1(b)]. A digital signal-processing board (dSPACE, DS1103) was used for data acquisition and control signal generator. The measuring data were acquired using real-time interface ControlDesk software (dSPACE) and linked to MATLAB for analysis throughout the experiment. For the actuation measurement, some IPMC samples with dimensions of 15 mm in length, 4 mm in width, and 0.34–0.37 mm in thickness were prepared. The experiments were carried out under a 5-V square-wave input and various actuation frequencies from 0.1 to 1 Hz. This experiment aims to characterize IPMC force and displacement responses under various actuation frequencies. The square-wave input signal was chosen in this experiment because it creates the greatest force and displacement, as well as the fastest response, in comparison with sinusoidal and sawtooth wave input signals. Fig. 2(a) shows that the displacement and blocking force of the IPMC actuator are inversely proportional to the actuation frequency, i.e., when we increase the actuation frequency,

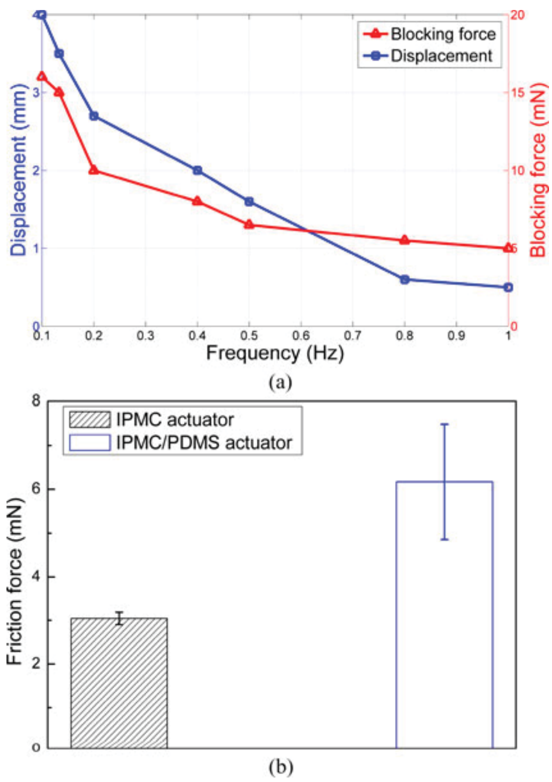

Fig. 2. (a) Response of IPMC under various input signals (5 V, 0.1–1 Hz). (b) Friction force of walking robot with and without PDMS coating.

the displacement and the blocking force of the IPMC actuator are decreased. At 0.1 Hz, our proposed IPMC actuators show 4 mm in displacement and 16 mN in blocking force, whereas the displacement and blocking force are decreased to 0.5 mm and 5 mN at 1 Hz, respectively. At a low actuation frequency, a small back relaxation was observed. This back relaxation can be explained by a loss in water molecules inside the membrane. In addition, since this thin IPMC (about 0.36 mm) has less absorbed water inside the ion exchange membrane than the thick one, back relaxation occurred quickly.

B. Enhancement of IPMC Leg Performance Using Polydimethylsiloxane Coating Method

In micro- and mesoscales, the surface friction force plays a very important role in the interactions between objects. Especially in a walking robot, the friction between the robot's legs and the ground decides the efficiency of the robot motion. In previous works, we designed a walking robot using two and four 1DoF legs and implemented the walking motion on many kinds of walking surfaces, such as paper, metal, plastic, glass. Finally, a Teflon surface was chosen for further walking tests, as it provided better walking results. In addition, when a robot was walking, it exhibited slipping, which causes lowed or disturbed locomotion. The loss of ground contact between the IPMC leg and the ground was the main reason for this problem.

In order to solve this slipping problem, we adopted a thin Polydimethylsiloxane (PDMS) polymer layer to cover the IPMC leg, which can easily bend and come in full contact with the walking plane, no matter how great the contact angle. PDMS is appropriate for use in this situation because of its flexible properties and ease of fabrication process. The dip coating method is used to coat the PDMS layer out of the IPMC actuator. First, a PDMS solution with a ratio of 10:1 Sylgard 184A, i.e., a silicone elastomer base, and Sylgard 184B, i.e., a silicone elastomer curing agent, was made. Then, the IPMC actuators were immersed in the PDMS solution to cover about 80% of the length of the IPMC, leaving 20% for attaching the electrodes. The IPMCs with the PDMS coating (called IPMC/PDMS) were hung in the oven at 80 °C for 1 h. In addition, IPMC actuators with a thin PDMS layer are reserved in the deionized water for the actuation test. The IPMC/PDMS were assembled in the robot, and the load cell (GSO-10, Transducer Techniques) was connected to the walking robot for the measurement of the friction and propulsion force, as shown in Fig. 1(c). The linear translational stage was adjusted to increase the tension on the wire that connects the load cell and the walking robot, until the robot starts to slide. At that moment, the maximum friction force between the robot leg and the ground can be measured and recorded. We repeated this experiment many times with IPMC/PDMS and IPMC actuators to compare their performances. The experimental results [see Fig. 2(b)] demonstrated that the walking robot using IPMC/PDMS showed greater friction force that that using IPMC alone. That is, the friction coefficient of IPMC/PDMS on the Teflon surface is about 0.456 on average, which is over twice the value of IPMC alone (0.21). They showed that an IPMC/PDMS actuator has better ground contact than that of IPMC itself, and therefore, slipping in the IPMC walking robot is reduced. Moreover, by coating a thin PDMS layer outside of the IPMC actuator, the ground contact was improved, the motion was not disturbed, and life time of the IPMC actuator in air conditioning was increased. Because the thin PDMS layer covers the micropores and cracks on the surface of the IPMC, it reduces significantly the leakage of water molecules out of the membrane in the actuation process.

III. Robot Design

A. Hardware Design

To date, the mechanical designs of the IPMC walking robots have been focused on a simple and lightweight robot structure using many lightweight materials and simple structures for the robot body, such as wood, plastic, composite, etc. It turns out it is very difficult to reduce the weight and complex connection between a large number of electrodes and control circuits on a robot's body. To solve this problem, a circuit board was used for the robot's body, upon which all the mechanics, electronics, and actuators were installed.

A 440-μm doubled-sided circuit board was used for this purpose, resulting in a weight of about 160 mg of the unpopulated board. Basically, the robot body was symmetrically designed to maintain the balance of the walking robot. Based on the experiences in our previous versions [13], modularity was the key of the system integration concept, which does not require a high degree of skill for the integration of mechanics and electronics. The modular design was also applied to the robot body

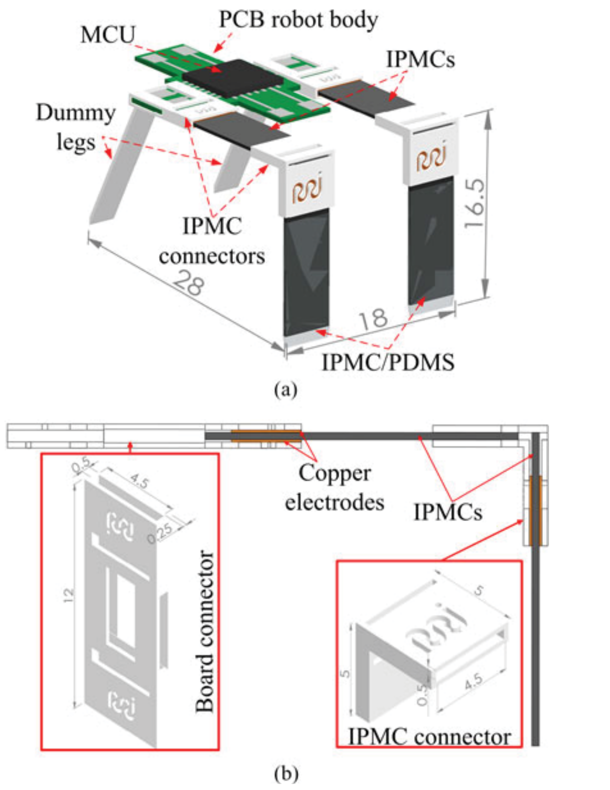

Fig. 3. (a) Design of IPMC walking robot. (b) Design structure of 2DoF leg.

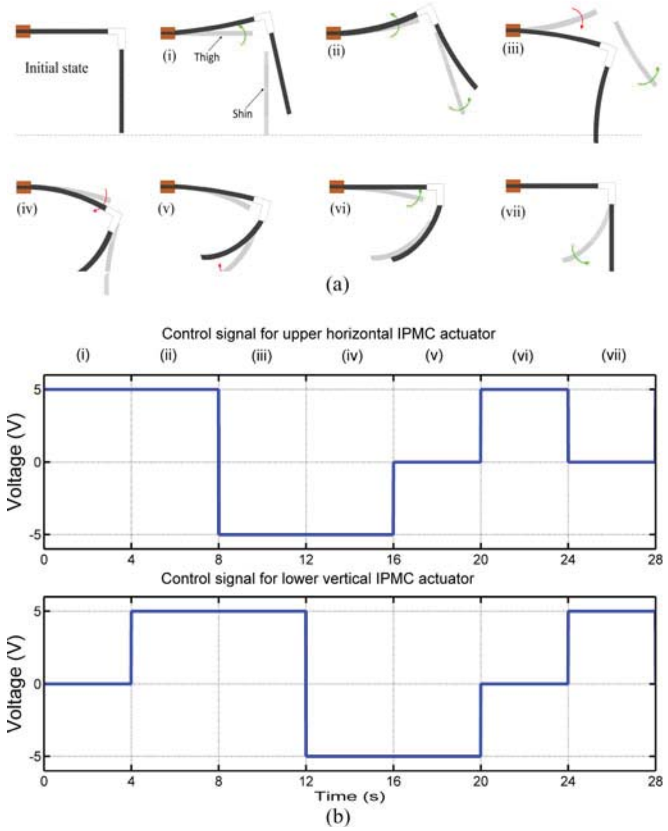

Fig. 4. (a) Locomotion of 2DoF leg. (b) Sequence control signal of 2DoF leg corresponding to part (i)–(vii) in part (a).

and 2DoF legs in order to facilitate rapid parametric testing of control circuit and actuators.

Fig. 3(a) shows the proposed IPMC walking robot, which consists of two 2DoF legs and a special board connector with two ABS plastic dummy legs. A distance (29 mm) between the front and rear legs was designed based on the experimental deformation data of a 2DoF leg to prevent bumping each other and to maintain the balance of the robot during the walking process. In order to provide 2DoFs for each leg, two IPMC actuators were conjoined perpendicularly as a shin and a thigh, which can show the swing and lift motions [see Fig. 3(b)]. Each IPMC actuator has the same size of $15\ \mathrm{mm} \times 4\ \mathrm{mm} \times 0.36\ \mathrm{mm}$ as those selected from previous experiments.

The horizontal IPMC actuator, the thigh, shows the lift motion to raise the leg from the walking surface. In addition, the vertical IPMC actuator, the shin, shows the swing motion to provide a locomotive stroke across the walking plane. In addition, the key to this 2DoF structure is that these two IPMC actuators can work independently or simultaneously. The combination of two IPMC actuators mimics the leg structure of the real insect to create a large bending displacement and to ensure the force to support and drive the robot.

For the connection of the IPMC actuator with the robot body, clamping devices were necessary, as their clamping pressures could provide a strong effect on the performance of the IPMC actuators. During the clamping process, the mechanical stiffness and the electrical contact resistance between the electrodes of the IPMC and the clamping device will be greatly changed, according to the changes in clamping pressures [12].Therefore, in bio-systems using IPMC as well as an IPMC robot, the clamping device, the electrodes that connect between the IPMC, and control system are important. They should simply attach the control wire to the IPMC without damage and ensure the optimal clamping pressure to obtain the largest bending deformation of the IPMC actuator. Fig. 3(b) illustrates two different kinds of connectors: an IPMC connector, which conjoins the thigh to the shin of the robot leg, a board connector, which connects the 2DoF leg module to the robot body. These two connectors were made of ABS plastic using a 3-D printer (Objet 30, Stratasys) with 0.1-mm accuracy. The gap (0.5 mm) in the connectors was designed for about a 360-μm thickness of the IPMC actuators to ensure a suitable clamping pressure was applied to the actuators. An 80-μm-thick copper tape was also used as electrodes to cover the inner wall of the connectors. An IPMC with a 360-μm thickness was inserted between two copper electrodes (160-μm thickness) inside the connector with a tolerance of $-20\ \mu$m. Through this design of the connection part, we cannot only execute easy assembly but also provide enough clamping pressure without damage to the IPMC surface.

Fig. 4(a) illustrates the walking procedure of 2DoF leg. The locomotion of the 2DoF leg was obtained by the combination of separate motions or simultaneous motions of the horizontal IPMC actuator (thigh) and the vertical IPMC actuator (shin). Based on the stage of the 2DoF leg, we could divide its motions in two phases: swing phase and stance phase. The swing phase is the stage in which the leg performs a vertical lift-off and moves forward (protraction motion), and the stance phase is the stage in which the leg has ground contact and bends backward to provide a locomotive stroke in the walking plane (retraction motion). In general, one walking cycle of a 2DoF leg can be decomposed into seven stages, as shown in Fig. 4(a), as follows:

(i) The leg starts from initial state, and then, the thigh starts to bend upward and lift the shin off the ground to avoid pushing the robot back with respect to the next foothold.

(ii) The shin starts to bend forward, while the thigh keeps bending upward to lift the shin. In this stage, the 2DoF leg shows the protraction motion that finishes the first swing phase and prepares for the next stance phase.

(iii) The thigh starts the stance phase by bending downward, while the shin is continuously bending forward to ensure full stroke in the next step.

(iv) The thigh and shin show simultaneously the retraction motions that provide the strongest stroke in this proposed locomotion with the largest displacement and greatest blocking force in order to push the robot forward.

(v) In this step, the shin keeps bending backward to finish the full stroke.

(vi), (vii) The thigh and shin move sequentially upward and forward to return back to initial state and finish the second swing phase of the 2DoFleg's locomotion.

Fig. 4(b) illustrates the control signal for two IPMC actuators to control the bending motions of the 2DoF leg corresponding to parts (i)–(vii) in Fig. 4(a). These signals are generated by a control circuit.

This proposed locomotion strongly promotes the performance of the 2DoF structure by a combination of simultaneous protraction and retraction motions of the thigh and shin to generate large displacement and sustain the blocking force for supporting and driving the walking robot. Therefore, it can enhance the performance of our walking robot. Based on the combination of the proposed structure and the proposed locomotion sequence, the 2DoF leg was tested through a series of experiments and testing methods, such as the blocking force test and the displacement test, to characterize the features of 2DoF leg in comparison with a 1DoF leg. The experimental setup for the2DoF leg is the same as that for a 1DoF leg, as described in part A of Section II. However, in the blocking force measurement of 2DoF leg, we reversely positioned the 2DoF leg and the load cell to measure the protraction motion. The purpose of this reverse is to avoid the gravitational effect.

The experiments were repeatedly implemented to compare the performance of this combination of the proposed structure, the locomotion sequence, and the driving voltages with the performance of the IPMC itself under a 5-V DC input signal. Compared with a 1DoF leg, Fig. 5 demonstrates the superior characteristics of the proposed structure of a 2DoF leg. It shows the strong increase in the displacement, which is around three times (10.125 mm) bigger than that of the IPMC itself (3.5 mm), as well as the light difference in the blocking force between the 2DoF leg (2.031gf) and 1DoF leg (2.3gf). These measurement results proved that the proposed walking mechanism using a 2DoF leg can enhance the performance of the walking robot through a strong increase in the displacement and sustainment of the locomotive power.

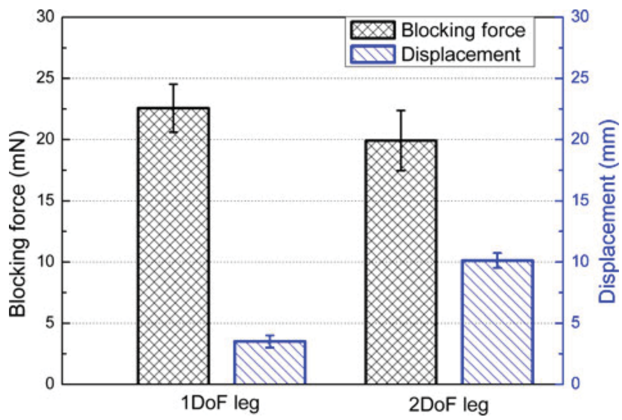

Fig. 5. Blocking force and displacement experimental results of 1DoF and 2DoF leg structures.

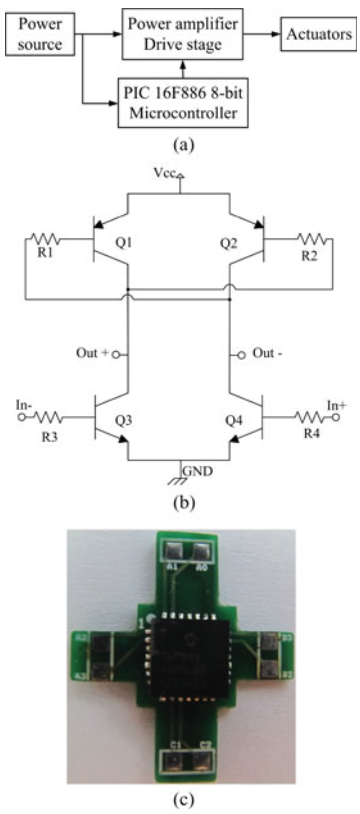

Fig. 6. (a) Schematic of the circuitry for the walking robot. (b) Detailed schematic of the drive stage for the IPMC actuator. (c) Populated PCB robot body.

B. Electronics Design

In order to minimize the size of the control system and the autonomous robot, a minicontroller must provide the following functions for a robot with up to four IPMC actuators: locomotion generator, drive stage, and programming interface. Fig. 6(a) shows the general schematic of the circuitry of the walking robot. The sequence control signals were created by a microcontroller and converted by a drive stage to drive multiple IPMC actuators. The proposed IPMC has absorbed a driving current of around 100 mA when it operates. The instant maximum current, around 200 mA, occurs when the voltage changes abruptly in a square-wave control signal. We design a drive stage using an edited H-bridge with bipolar junction transistors PNP 2SB1219 (Q1, Q2) and NPN 2SD1820 (Q3, Q4, Panasonic). In Fig. 6(b), the drive transistor resistors are designed as $R1 = R2 = R3 = R4 = 470\ \Omega$, in order to provide the maximum supply current of around 300 mA. The drive stage amplifies the current of the sequence control signal from microcontroller (PIC16F886, 8 bit, manufactured by Microchip Technology Inc.), but maintains the voltage gain as one. Four of these drive stages are used to drive four actuators individually. All the selected electrical components are the smallest surface mount components in the market in order to optimize the size and weight of the circuit. Finally, through manual soldering, we created a 320-mg populated circuit board [see Fig. 6(c)].

IV. Modeling

A. Dynamic Model of PVDF/PVP/PSSA-Based IPMC Actuator

In previous works [13], [14], the electrical dynamics of a Nafion-based IPMC actuator were fully investigated to obtain the deformation generated within the IPMC. However, the dynamics models for other membrane-based IPMC actuators have not been reported yet. Especially, the PVDF/PVP/PSSA-blend-membrane-based IPMC actuator exhibits higher tip displacement and greater blocking force than a Nafion-based IPMC actuator. In this study, we try to investigate the dynamic model for our proposed blend membrane-based IPMC actuator by applying our membrane parameters to the physics-based model. A transfer function relating the free tip displacement of an IPMC actuator *δ(L,s)* to the actuation voltage *V(s)*was introduced when the beam dynamics were ignored [14], $H(s) = \delta(L,s)/V(s)$.

$$H(s) = -\frac{L^2 k_0 W K \kappa_e \left(\gamma(s) - \tanh(\gamma(s))\right)}{2YI\left(\gamma(s)s + K\tanh(\gamma(s))\right)} \left(\frac{2X(s)}{1 + r_2'\theta(s)/W}\right) \tag{1}$$

with

$$X(s) = \frac{1 - \mathrm{sech}\left(\sqrt{B(s)}L\right) - \tanh\left(\sqrt{B(s)}L\right)\sqrt{B(s)}L}{B(s)L^2}$$

$$\theta(s) = \frac{sW\kappa_e\gamma(s)(s+K)}{h\left(s\gamma(s) + K\tanh(\gamma(s))\right)}$$

$$B(s) = \sqrt{r_1\left(\frac{\theta(s)}{(1 + r_2\theta(s))} + \frac{2}{R_p}\right)}$$

$$\gamma(s) = \sqrt{\frac{s+K}{d}}$$

$$K = \frac{F^2 d C^-}{\kappa_e RT}\left(1 - C^-\Delta V\right)$$

TABLE I
Parameters for Actuation Model

T	F	R	R_p'
300 K	96485 C/mol	8.3143 J/mol	0.0307 Ωm^2
r_1'	r_2'	4.181×10^8 Pa	C^-
24.05 Ω	$2.73 \times 10^{-8}\ \Omega\text{m}$	4.181×10^8 Pa	1091 mol/m^3
h	d	κ_e	k_0
180 μm	4.914×10^{-9} m^2/s	1.2309×10^{-5} F/m	0.454 J/C

where *L*, *W*, and *h* are the length, width, and half thickness, respectively, of the IPMC actuator, and k_0 is an electromechanical coupling constant, κ_e is the effective dielectric constant of the polymer, *d* is the ionic diffusivity, *R* is the gas constant, *F* is Faraday's constant, *T* is the absolute temperature, C^- is the anion concentration, ΔV is the volumetric change, r_1 is the electrode resistance per unit length in the length direction, r_2 is the electrode resistance per unit length in the thickness direction, r_2' is the surface resistance per $\{$unit length $*$ unit width$\}$ in the thickness direction, and R_p is the through-polymer resistance per unit length. In addition, *Y* is the effective Young's modulus of the IPMC, and $I = 2Wh^3/3$ is the moment of inertia of the IPMC actuator.

The transfer function *H(s)* was described earlier where the beam dynamic was ignored. Then, regarding the bending case, in order to accommodate the vibration dynamics of the IPMC strip, a transfer function *G(s)* was multiplied by *H(s)*. The output of *G(s)* represented the bending displacement (as that of *H(s)* does). At low actuation frequencies, the IPMC actuator resembled well-behaved linear time-invariant second-order systems.

$$G(s) = \frac{c}{s^2 + as + b} \tag{2}$$

with

$$a = 2\omega_n\zeta;\ b = \omega_n^2;\ c = Ab$$

where ω_n is the natural frequency of the IPMC beam, ζ is the damping ratio, and *A* is the dc gain.

Table I lists the parameters obtained for the actuation model. Among them, gas constant *R* and Faraday's constant *F* are the physical constants. The absolute temperature, *T*, the effective Young's modulus *Y*, the surface resistance r_1 in the *z*-direction, and through-polymer resistance R_p are directly measured from our proposed PVDF/PVP/PSSA-based IPMC actuator. A nonlinear fitting process was used to identify the other parameters, such as the diffusion coefficient *d*, the dielectric constant κ_e, the anion concentration C^-, and the surface resistance densityr_2' in the *x*-direction based on the empirical impedance response of an IPMC actuator with dimensions $15\,\text{mm} \times 4\,\text{mm} \times 0.36$ mm. Last, k_0 are simply considered as the gain parameter in the actuation model, which is identified as $k_0 = 0.454$ J/C using the actuation response of the IPMC actuator under a sinusoidal input voltage. The parameters are listed in Table I, where the value of C^- is the same as [14]. However, *d* and κ_e are different from those in [14].

Then, the natural frequency ω_n and damping ratio ζ in *G(s)*were identified in the active state based on the bending displacement $\delta(t)$ at the free end of the IPMC actuator by applying the sinusoidal actuation signal *V*(*t*) with an amplitude of 1 V and frequencies from 0.02 to 20 Hz. The estimation method is described in the following.

$$T(s) = H(s)G(s) = \frac{a_n s + b_n}{s^2 + c_n s + d_n} \frac{c}{s^2 + as + b} = \frac{\delta(s)}{V(s)} \tag{3}$$

$$\Rightarrow \frac{c}{s^2 + as + b} = \frac{s^2\delta(s) + c_n s\delta(s) + d_n\delta(s)}{a_n sV(s) + b_n V(s)}. \tag{4}$$

Denote that:

$$\begin{aligned} y(s) &= s^2\delta(s) + c_n s\delta(s) + d_n\delta(s) \\ z(s) &= a_n sV(s) + b_n V(s). \end{aligned} \tag{5}$$

Take the inverse Laplace transform of the aforementioned equation, given as

$$\begin{aligned} y(t) &= \ddot{\delta}(t) + c_n\dot{\delta}(t) + d_n\delta(t) \\ z(t) &= a_n\dot{V}(t) + b_n V(t). \end{aligned} \tag{6}$$

Then, by substituting (5) into (4), take the inverse Laplace transform as

$$\frac{1}{c}\ddot{y}(t) + \frac{a}{c}\dot{y}(t) + \frac{b}{c}y(t) = z(t) \tag{7}$$

where $a_n, b_n, \text{and}\, c_n$ are known parameters, as calculated by applying the identified parameters in Table I into (1). The matrices $\ddot{y}(t)$, $\dot{y}(t)$, *y(t)*, and *z(t)* are n×1 matrices, which were calculated from the input voltage *V(t)* and output displacement $\delta(t)$ of the IPMC actuator. Then, the parameters *a*, *b*, and *c* can be easily calculated by applying the Moore-Penrose pseudoinverse (*pinv* in MATLAB) into (7); *G(s)* will have a dc gain (*A*) of 1.347.

Finally, the fourth-order model for the overall actuation response for our proposed PVDF/PVP/PSSA-based IPMC actuator can be denoted as

$$T(s) = \frac{0.004703\ \mathrm{s} + 0.01047}{s^2 + 14.52\ \mathrm{s} + 10.04} \cdot \frac{1338.3}{s^2 + 5.7114\ \mathrm{s} + 993.5}. \tag{8}$$

From Fig. 7, we can see that the actuation model matches closely the empirical response of the IPMC actuator. This actuation model will be used for a database of kinematic models of 2DoF IPMC legs in the next section.

B. Kinematic Model of 2DoF IPMC Leg

In an earlier work [15], Nabako *et al.* introduced a kinematic model for a 3DoF IPMC robot manipulator, but they assumed that the link was bent with a constant curvature, which is correct with a small bending angle in a real IPMC actuator. In this study, in order to realize the motion curve of our proposed 2DoF leg, we proposed a kinematic model for this structure using the curvature generated from our actuation model of a PVDF/PVP/PSSA-based IPMC actuator. First, a kinematic model for an IPMC

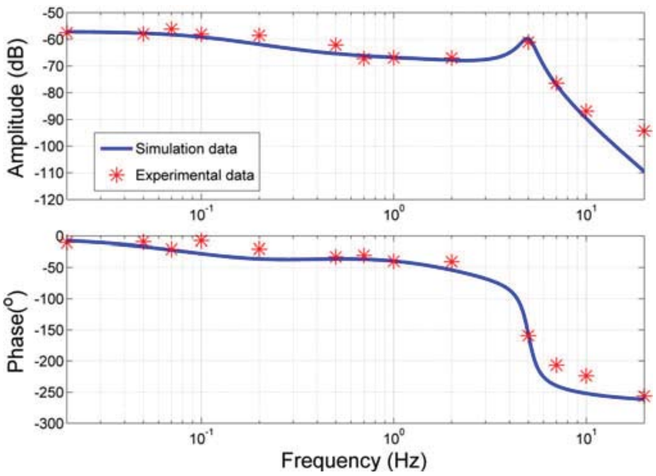

Fig. 7. Comparison of the measured actuation response with the simulation of actuation model.

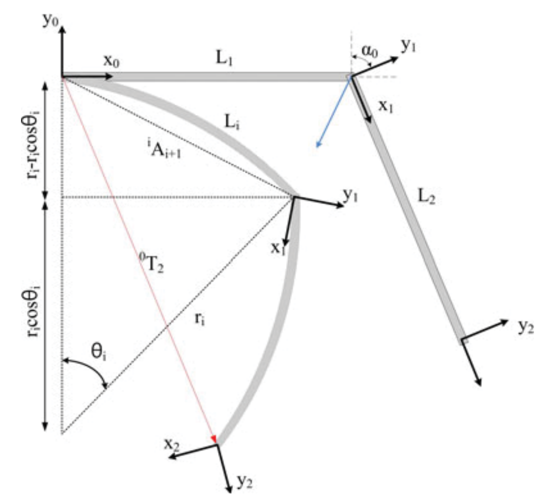

Fig. 8. Kinematic modeling of 2DoF leg's bending motion.

actuator was introduced, which is similar to the conventional serial link robot manipulator, but the key difference is that the link itself shows that the bending motion consists of a rotation and translation in one IPMC actuator. Fig. 8 illustrates the kinematic of an IPMC bending motion. The whole kinematic model was considered in 2-D spaces because of its structure, which was presented in Section III. The coordinate systems (x_i, y_i), $(i = \{0, 1, 2\})$ are defined and placed at corresponding origin and joints (see Fig. 8). The bending motion of an IPMC actuator can be represented in rotation terms and translation terms, as follows:

$${}^iR_{i+1} = [{}^iX_{i+1} \;\; {}^iY_{i+1}] = \begin{bmatrix} \cos(\theta_i + \alpha_i) & -\sin(\theta_i + \alpha_i) \\ \sin(\theta_i + \alpha_i) & \cos(\theta_i + \alpha_i) \end{bmatrix} \tag{9}$$

$$^{i}P_{i+1} = \begin{bmatrix} r_i \sin(\theta_i) \\ r_i - r_i \cos(\theta_i) \end{bmatrix} = \begin{bmatrix} \frac{L_i}{\theta_i} \sin(\theta_i) \\ \frac{L_i}{\theta_i}(1 - \cos(\theta_i)) \end{bmatrix} \tag{10}$$

where $^{i}R_{i+1}$ presents the rotation term from joint i^{th} to $i^{\text{th}} + 1$, and $^{i}P_{i+1}$ denotes the translation term from joint i^{th} to $i^{\text{th}} + 1$. As well, L_i is the length of the IPMC actuator and α_i is the fixed bending angle between link i^{th} *to* $i^{\text{th}} + 1$. In addition, θ_i is the curvature of the link i^{th}, which is calculated from the tip displacement in the actuation model of our proposed IPMC actuator, as follows:

$$\delta = r(1 - \cos(\theta)) = \frac{L}{\theta}(1 - \cos(\theta)). \tag{11}$$

Applying the Taylor expansion for trigonometric function, we could obtain the approximate relationship between displacement and bending curvature as

$$\delta = \frac{L}{\theta}\left[1 - \left\{1 - \frac{1}{2!}(\theta)^2\right\}\right] = \frac{L\theta}{2}. \tag{12}$$

A homogenous transformation matrix $^{i}A_{i+1}$ from joint ith to $i\text{th} + 1$ is written as

$$^{i}A_{i+1} = \begin{bmatrix} \cos(\theta_i + \alpha_i) & -\sin(\theta_i + \alpha_i) & \frac{L_i}{\theta_i}\sin(\theta_i) \\ \sin(\theta_i + \alpha_i) & \cos(\theta_i + \alpha_i) & \frac{L_i}{\theta_i}(1 - \cos(\theta_i)) \\ 0 & 0 & 1 \end{bmatrix}. \tag{13}$$

Then, the kinematics for our proposed 2DoF leg was introduced based on the analysis of an IPMC bending motion. In our 2DoF structure, the shin is fixed perpendicular to the thigh [see Fig. 3(b)]; thus, $\alpha_1 = -\pi/2, \alpha_2 = 0$. The lengths (L_1, L_2) of the links in this kinematic model are same as the lengths of IPMC actuators used in Section II ($L = 15$ mm). The transformation matrix that shows the bending motion of 2DoF leg was calculated by multiplying each transformation matrix from the base to the end effector point (see Fig. 8), using

$$^{0}T_2 = {}^{0}A_1 {}^{1}A_2. \tag{14}$$

Finally, the position vector of the end effector ($P_E = (P_{Ex}, P_{Ey})^T$), which shows the motion curve of the 2DoF leg can be obtained from the following equation, as follows:

$$P_{Ex} = \frac{L}{\theta_1\theta_2}(-\theta_1\cos(\theta_1 + \theta_2) + \theta_1\cos(\theta_1) + \theta_2\sin(\theta_1)) \tag{15}$$

$$P_{Ey} = \frac{L}{\theta_1\theta_2}(\theta_2 - \theta_1\sin(\theta_1 + \theta_2) - \theta_2\cos(\theta_1) + \theta_1\sin(\theta_1)). \tag{16}$$

V. Experimental Verification

In order to verify whether the theoretical displacement based on the actuation model for our proposed IPMC is reasonable, the tip displacements of various PVDF/PVP/PSSA-based IPMC actuators have been measured under sinusoidal voltage. Fig. 9 shows the tip displacement versus time of the IPMC actuators when a sinusoidal voltage with an amplitude of 1 V, frequency of 0.05 Hz was applied. The tip displacements between the simulation and experimental data were closely matched. However, the experimental data shows a small drift up from the central line due to the different electrode coating between two surfaces of the IPMC actuators leading to different stiffness and electrical properties between these two surfaces. In addition, a small difference in the phase was also observed. We estimated that this difference is due to the inertia and damping effects, which are not perfectly fitted to the real values of the IPMC actuator, as showed in frequency response in Fig. 7. Then, to verify the capabilities of our proposed 2DoF leg structure in controlling the motion curve and ground contact, we have measured the displacement of this structure under a sequence control signal in Fig .4(b).

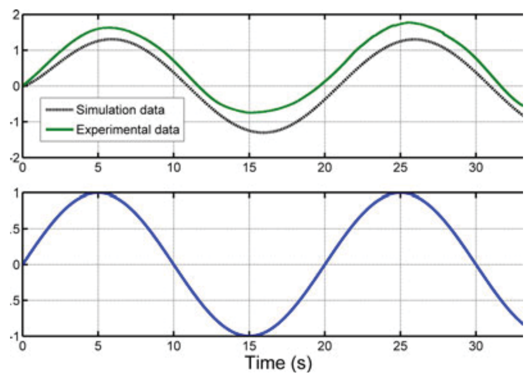

Fig. 9. Theoretical and experimental tip displacement of IPMC actuator versus time when a sinusoidal voltage (1 V, 0.05 Hz) is applied.

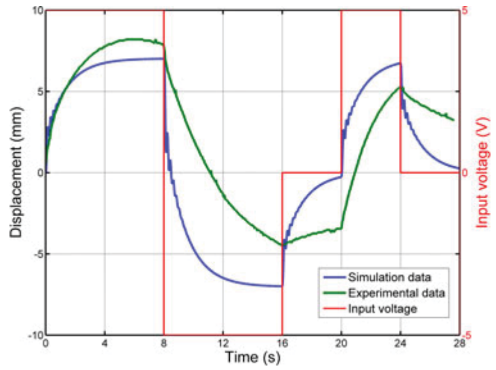

Fig. 10. Theoretical and experimental displacements of upper leg under sequence control signal.

The 2DoF leg was fastened to the clamping device and connected to the control circuit. A camera was fixed perpendicular to this 2DoF IPMC leg at a distance of 60 mm to record its motion. Two red markers were attached to each joint for tracking the motion curve of the thigh and shin. Fig. 10 illustrates the experimental displacement of the upper leg, which was extracted using video motion tracking, in comparison with the simulation displacement, which is predicted by actuation model under sequence control signal of 5 V with intervals of 4 s. We could see the similarity in shape between the measurement and simulation results. However, at times 16–20 s and 24–28 s, there

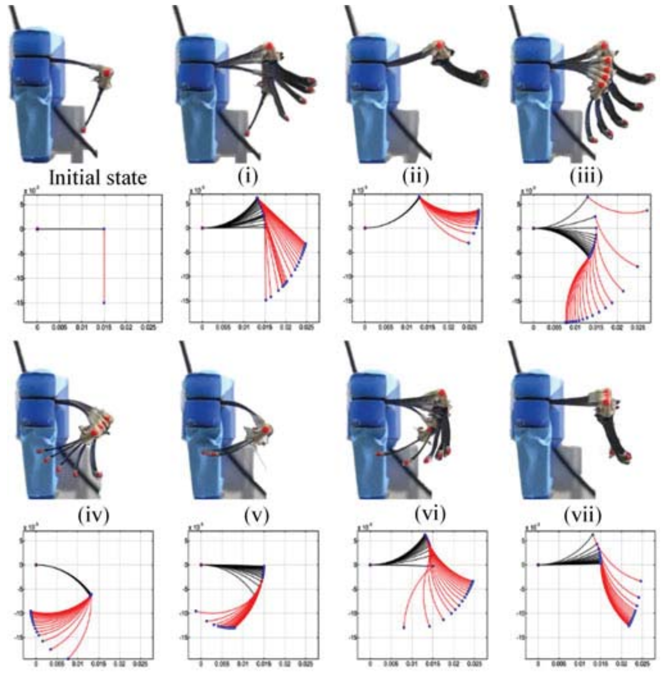

Fig. 11. Comparison of motion tracking and simulation data of the 2DoF leg following the time sequence.

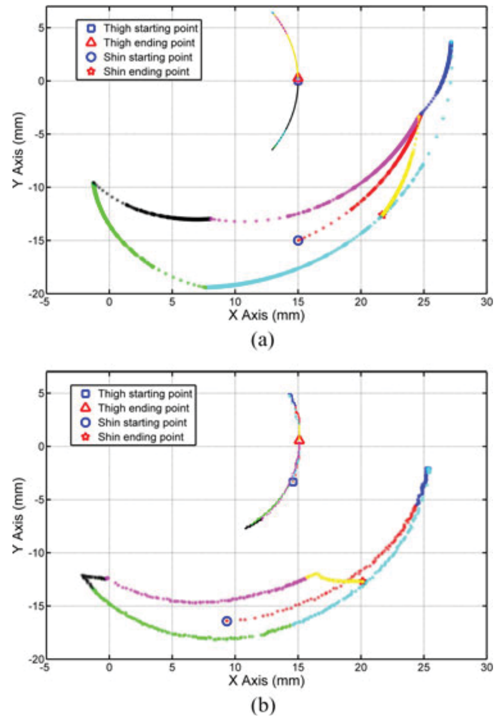

Fig. 12. Comparison of (a) simulation data and (b) motion tracking of 2DoF leg. With colors of red, blue, cyan, green, black, magenta, and yellow corresponding to part (i)–(vii).

are big differences between the measurement and simulation results where the simulation results move fast to the initial position (zero), while the measurement shows a slow back relaxation when the input signal becomes zero. This difference could occur because the back relaxation of the actuation model has not yet been considered. In addition, this can be the limitation of this actuation model on which further researches needs to focus.

Then, the theoretical displacement of the upper and lower legs of 2DoF legs, generated by actuation model, were used as the input for the kinematic model of the 2DoF leg after being converted into the bending curvature based on (13). Fig. 11 demonstrates the agreement in the locomotion of the 2DoF leg between the simulation and experimental data, following the time sequence. Parts (i)–(vii) in Fig. 11 are the step responses of the 2DoF leg, which describe the step-by-step locomotion of 2DoF leg in the real world, as corresponding to an input sequence 5 V, intervals of 4 s. They also prove the possibility of this desired driving signal [see Fig. 4(b)] for obtaining our proposed locomotion [see Fig. 4(a)]. However, there are some differences between the measurement and simulation in Fig. 11 that we can easily observe, including in the initial state, as well as in steps (v) and (vii). The differences in the initial state of the measurement data and simulation, wherein the upper and lower legs are not in a perpendicular position, are due to the shape of the IPMC itself and gravity. The differences in steps (v) and (vii) are already explained in Fig. 10.

Fig. 12 illustrates the full steps (one cycle) locomotion of a 2DoF leg based on the above step-by-step analysis. The theoretical displacement of the 2DoF leg was presented in Fig. 12(a), while (b) presented the experimental displacement using a video processing motion tracking method. Each step in these two figures was distinguished by a different color. Step (a) starts with a red color and continues with blue, cyan, green, black, magenta, and yellow that correspond to steps (ii) though (vii) in robot locomotion. In this figure, once again we could see the agreement between the theoretical and experimental motion curves of the 2DoF leg. Other than a small drift down, the simulation result of the upper leg closely matched the experimental result. The horizontal displacement of the end effector of the 2DoF leg is 27.6 mm in the experiment results and 28.3 mm in the simulation results. This result proves that we can generate the effective motion curve using this proposed the 2DoF IPMC leg structure.

TABLE II
DISPLACEMENT DATA OF 2DOF LEG

Interval (s)	Displacement (mm)
5	26.7
4	27.6
3	27
2	20.1
1	19.8
0.5	10.5
0.4	9.6
0.3	8.3
0.2	7
0.1	4

Additional experiments were carried out to characterize the 2DoF IPMC leg performance by changing the time interval between each step. Table II shows the results of these experiments. Many different interval times were chosen to test the

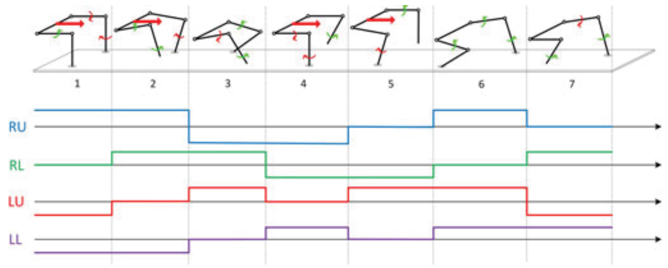

Fig. 13. Locomotion of the walking robot using two 2DoF legs structure and corresponding sequence control signal. RU stands for right upper leg, RL is right lower leg, LU is left upper leg, and LL is left lower leg.

performance of this proposed structure, including 5, 4, 3, 2, 1, 0.5, 0.4, 0.3, 0.2, and 0.1 s. According to the experimental results in Table II, we could conclude that the interval times design the speed as well as the displacement of this structure. A longer interval time generates a larger tip displacement and a slower speed of the 2DoF IPMC leg and vice versa. With this proposed structure and locomotion, we could not only generate the effective motion curve of the robot's legs, but we could also easily control it by changing the interval between each step. In addition, our proposed models can be used to predict the motion curve of our 2DoF leg with a new interval time or new control sequence signal for design or optimization the locomotion of the walking robot. The developed modeling framework may be useful for the control of the walking robot to meet a trade-off between tip displacement and locomotion speed to obtain the best performance of the walking robot.

Finally, we fabricated a terrestrial walking robot prototype using two 2DoF legs and two dummy legs with a weight of 1.2 g, 28 mm in length, 18 mm in width, and 16.5 mm in height. Based on the proposed locomotion and performance of the 2DoF legs, we designed the locomotion for this walking robot using two 2DoF legs and two dummy legs by applying the proposed locomotion sequence for the 2DoF legs and changing the phase shift between the left and right legs, as shown in Fig. 13. The right 2DoF leg is kept at the same locomotion with a phase shift of zero, while the left has a three-step delay in comparison with the right leg. These two 2DoF IPMC legs alternatively touched the ground and pushed the robot body forward, mimicking real insect locomotion. This proposed locomotion for the walking robot using two 2DoF legs and two dummy legs has four instead of seven steps (step: first, second, fourth, fifth) that can generate the locomotive power to support and drive the robot forward, as shown in Fig. 13.

The walking test of this walking robot was implemented on a flat Teflon surface using the locomotion sequence described above under a control sequence voltage of a 5-V amplitude and 2-s intervals. In Fig. 14, the walking robot travelled 20 mm on the Teflon surface in 50 s, corresponding to three cycles of the sequence control signal (see Fig. 13) or 25 walking steps, resulting in a walking speed 0.4 mm/s. The walking robot performed the desired motion curve and walked smoothly throughout the performance. However, we observed a drift in the 2DoF leg out of the initial state, which changes the motion curve and limits the lifetime of 2DoF leg. The reasons for this problem have been

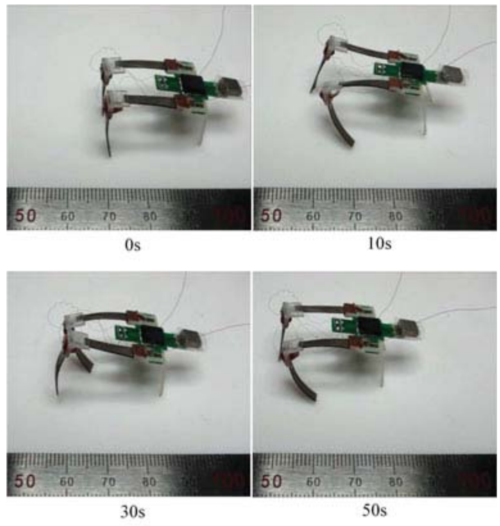

Fig. 14. Frame capture walking motion of the walking robot using 2DoF legs under sequence control signal 5 V, interval 2 s.

shown and discussed earlier through the comparison between the simulation and experimental data (see Figs. 9 and 10).

VI. Conclusion

We have presented the design of a terrestrial walking robot; a 1.2-g walking robot manufactured using a two 2DoF leg structure with a PVDF/PVP/PSSA-based IPMC actuator. The main contributions of this study are in the structure design, modeling, and demonstration of 2DoF legs capable of controlling motion curves. The bending motion curve of 2DoF leg was modeled by incorporating IPMC actuation dynamics into the kinematics of 2DoF IPMC leg structure. The model was verified in experiments on 2DoF leg different actuation frequencies and it showed a close agreement between the theoretical predictions and experimental data. The developed modeling framework may be useful for the control of robot locomotion to meet a tradeoff between displacement and locomotion speed in order to obtain the best performance of the robot. In addition, the models can be used to predict the leg performance for the design optimization of the leg through changing some designed parameters in the model, such as actuator length and fixed bending angle. The proposed IPMC actuator with a small size proved its ability to support and drive the walking robot. Future works may address the limitations mentioned in Section V, including enhancing the IPMC's characteristics for a longer lifetime, a steadier performance in air conditioning, and orientation and position control for this proposed 2DoF IPMC leg structure. Another future topic includes the integration of sensors and power that can create a fully autonomous walking robot in the next generation.

References

[1] M. Shahinpoor, Y. Bar-Cohen, J. O. Simpson, and J. Smith, "Ionic polymer-metal composites (IPMCs) as biomimetic sensors, actuators and artificial muscles—A review," *Smart Mater. Struct.*, vol. 7, no. 6, pp. R15–R30, 1998.

[2] V. Panwar, K. Cha, J. O. Park, and S. Park, “High actuation response of PVDF/PVP/PSSA based ionic polymer metal composites actuator,” *Sens. Actuators B, Chem.*, vol. 161, no. 1, pp. 460–470, 2012.

[3] C. Bonomo, L. Fortuna, P. Giannone, and S. Graziani, “A method to characterize the deformation of an IPMC sensing membrane,” *Sens. Actuators A, Phys.*, vol. 123, pp. 146–154, 2005.

[4] M. Shahinpoor and K. J. Kim, “Ionic polymer-metal composites: I. Fundamentals,” *Smart Mater. Struct.*, vol. 10, no. 4, pp. 819–833, 2001.

[5] V. Panwar, B. S. Kang, J. O. Park, and S. H. Park, “New ionic polymer–metal composite actuators based on PVDF/PSSA/PVP polymer blend membrane,” *Polym. Eng. Sci.*, vol. 51, pp. 1730–1741, 2011.

[6] M. J. D. Otis, “Electromechanical characterization and locomotion control of IPMC BioMicroRobot,” *Adv. Mater. Sci. Eng.*, vol. 2013, pp. 683041-1–683041-17, 2013.

[7] Y. C Chang and W. J. Kim, “Aquatic ionic-polymer-metal-composite insectile robot with multi-DOF legs,” *IEEE/ASME Trans. Mechatronics*, vol. 18, no. 2, pp. 547–555, Apr. 2013.

[8] S. Guo, L. Shi, N. Xiao, and K. Asaka, “A biomimetic underwater microrobot with multifunctional locomotion,” *Robot. Auton. Syst.*, vol. 60, no. 12, pp. 1472–1483, 2012.

[9] N. K. Tien, D. Hwang, S. Jung, S. Y. Ko, J. O. Park, and S. Park, “Development of bio-inspired walking microrobot using PVDF/PVP/PSSA-based IPMC actuator,” in *Proc. IEEE Int. Conf. Mechatronics Autom.*, 2014, pp. 49–54.

[10] V. Panwar, C. Lee, S. Y. Ko, J. O. Park, and S. Park, “Dynamic mechanical, electrical, and actuation properties of ionic polymer metal composites using PVDF/PVP/PSSA blend membranes,” *Mater. Chem. Phys.*, vol. 135, no. 2, pp. 928–937, 2012.

[11] V. Panwar, S. Y. Ko, J. O. Park, and S. Park, “Enhanced and fast actuation of fullerenol/PVDF/PVP/PSSA based ionic polymer metal composite actuators,” *Sens. Actuators B, Chem*, vol. 183, pp. 504–517, 2013.

[12] H. Moeinkhah, J. Y. Jung, J. H. Jeon, A. Akbarzadeh, J. Rezaeepazhand, K. C. Park, and I. K. Oh, “How does clamping pressure influence actuation performance of soft ionic polymer–metal composites?” *Smart Mater. Struct.*, vol. 22, no. 2, art. no. 025014, 2013.

[13] S. Nemat-Nasser and J. Y. Li, “Electromechanical response of ionic polymer-metal composites,” *J. Appl. Phys.*, vol. 87, no. 7, pp. 3321–3331, 2000.

[14] Z. Chen and X. Tan, “A control-oriented and physics-based model for ionic polymer-metal composite actuators,” *IEEE/ASME Trans. Mechatronics*, vol. 13, no. 5, pp. 519–529, Oct. 2008.

[15] Y. Nakabo, T. Mukai, and K. Asaka, “Kinematic modeling and visual sensing of multi-DOF robot manipulator with patterned artificial muscle,” in *Proc. IEEE Int. Conf. Robot. Autom.*, 2005, pp. 4315–4320.

Kim Tien Nguyen received the B.S. degree in mechanical engineering from the Hochiminh University of Technology and Education, Hồ Chí Minh, Vietnam, in 2012 and the M.S. degree in mechanical engineering from Chonnam National University, Gwangju, Korea.

His research interests include microactuator/robot, and advanced robotics.

Seong Young Ko received the B.S., M.S., and Ph.D. degrees from the Department of Mechanical Engineering, Korea Advanced Institute of Science and Technology (KAIST), Daejeon, Korea, in 2000, 2002, and 2008, respectively.

In 2008, he was a Postdoctoral Researcher in the Department of Electrical Engineering, KAIST, and from 2009 to 2011, he was a Research Associate in the Mechatronics-In-Medicine Laboratory, the Department of Mechanical Engineering, Imperial College, London, U.K. Since October 2011, he has been an Assistant Professor in the School of Mechanical Engineering, Chonnam National University, Gwangju, Korea. His research interests include medical robotics, human–robot interaction, and intelligent control.

Jong-Oh Park received the B.S. from the Department of Mechanical Engineering, Yonsei University, Seoul, Korea in 1978, M.S. degrees from the Department of Mechanical Engineering, Korea Advanced Institute of Science and Technology, Daejeon, Korea in 1981, and the Ph.D. degree in 1987 in robotics from Stuttgart University, Stuttgart, Germany.

From 1982 to 1987, he worked as a Guest Researcher at Fraunhofer - Gesellschaft Institut fur Produktions technik und Automatisierung, Germany. He worked as a Principal Researcher in the Korea Institute of Science and Technology, Seoul, Korea, from 1987 to 2005. In 2005, he moved to Chonnam National University, Gwangju, Korea, where he is now a Full Professor of the School of Mechanical Engineering and a Director of the Robot Research Initiative. His research interests include biomedical microrobot, medical robot, and service robot.

Sukho Park (M’13) received the B.S. degree in 1993, the M.S. degree in 1995, and the Ph.D. degree in 2000, all in mechanical engineering from the Korea Advanced Institute of Science and Technology, Daejeon, Korea.

From 2000 to 2004, he worked as a Senior Research Engineer at LG Electronics Production Research Center, Korea. From 2004 to 2006, he worked as a Senior Researcher of Micro system Research Center, Korea Institute of Science and Technology, Seoul, Korea. In 2006, he moved to Chonnam National University, Gwangju, Korea, where he is currently an Associate Professor of the School of Mechanical Engineering and a Section Head of the Robot Research Initiative. His research interests include microactuator/robot and micromanipulation for biomedical instrumental applications.